Naval Surface Warfare Center
Carderock Division
West Bethesda, MD 20817-5700

NAVSEA
WARFARE CENTERS
Carderock Division

NSWCCD-50-TR–2012/043 December 2012
Hydromechanics Department Report

Joint High Speed Sealift (JHSS) Segmented Model Test Data Analysis and Validation of Numerical Simulations

By
Dominic Piro, Kyle A. Brucker, Thomas T. O'Shea, Donald Wyatt, Douglas Dommermuth, William R. Story, Edward A. Devine, Ann Marie Powers, Thomas C. Fu, and Anne M. Fullerton

Approved for public release; distribution unlimited.

REPORT DOCUMENTATION PAGE

Form Approved
OMB No. 0704-0188

Public reporting burden for this collection of information is estimated to average 1 hour per response, including the time for reviewing instructions, searching existing data sources, gathering and maintaining the data needed, and completing and reviewing this collection of information. Send comments regarding this burden estimate or any other aspect of this collection of information, including suggestions for reducing this burden to Department of Defense, Washington Headquarters Services, Directorate for information Operations and Reports (0704-0188), 1215 Jefferson Davis Highway, Suite 1204, Arlington, VA 22202-4302. Respondents should be aware that notwithstanding any other provision of law, no person shall be subject to any penalty for failing to comply with a collection of information if it does not display a currently valid OMB control number. **PLEASE DO NOT RETURN YOUR FORM TO THE ABOVE ADDRESS.**

1. REPORT DATE *(DD-MM-YYYY)*	2. REPORT TYPE	3. DATES COVERED *(From - To)*
December 2012	Final	Jan 2011-Dec 2012

4. TITLE AND SUBTITLE
Joint High Speed Sealift (JHSS) Segmented Model Test Data Analysis and Validation of Numerical Simulations

5a. CONTRACT NUMBER
N0001411WX21557

5b. GRANT NUMBER

5c. PROGRAM ELEMENT NUMBER

6. AUTHOR(S)
Dominic Piro, Kyle A. Brucker, Thomas T. O'Shea, Donald Wyatt, Douglas Dommermuth, William R. Story, Edward A. Devine, Ann Marie Powers, Thomas C. Fu, and Anne M. Fullerton

5d. PROJECT NUMBER

5e. TASK NUMBER

5f. WORK UNIT NUMBER
11-1-5800-390-10

7. PERFORMING ORGANIZATION NAME(S) AND ADDRESS(ES) AND ADDRESS(ES)

Naval Surface Warfare Center
Carderock Division
9500 Macarthur Boulevard
West Bethesda, MD 20817-5700

8. PERFORMING ORGANIZATION REPORT NUMBER

NSWCCD-50-TR-2012/XXX

9. SPONSORING / MONITORING AGENCY NAME(S) AND ADDRESS(ES)
Paul Hess
Office of Naval Research
845 N. Randolph Street
Building 875
Arlington, VA 22203

10. SPONSOR/MONITOR'S ACRONYM(S)
ONR

11. SPONSOR/MONITOR'S REPORT NUMBER(S)

12. DISTRIBUTION / AVAILABILITY STATEMENT Approved for public release; distribution unlimited.

13. SUPPLEMENTARY NOTES

14. ABSTRACT

The Joint High Speed Sealift (JHSS) segmented model (Model 5663) tests performed in 2007 at Naval Surface Warfare Center, Carderock Division (NSWCCD) were designed to provide a large data set for validation of numerical simulations. The segmented model had a scaled longitudinal stiffness in bending and torsion provided by an aluminum backspline. The hull of the model was cut into segments to lessen the stiffness effects of the shell. The model was self-propelled and steered during data collection. Preliminary validation work performed soon after the experiments with LAMP (Large Amplitude Motions Program) and Numerical Flow Analysis (NFA) showed favorable results. Additionally, the segmented model provided structural loading results that were used to understand hydroelastic phenomena such as springing and whipping. A study of the irregular seas cases showed that springing does not have a large effect on the JHSS model. The whipping response was explored for regular seas runs, with some cases showing significant loads on the ship. Efforts to understand

15. SUBJECT TERMS

16. SECURITY CLASSIFICATION OF:			17. LIMITATION OF ABSTRACT	18. NO. OF PAGES	19a. RESPONSIBLE PERSON
a. REPORT	b. ABSTRACT	c. THIS PAGE		30+vi	Anne Fullerton
UNCLASSIFIED	UNCLASSIFIED	UNCLASSIFIED			19b. TELEPHONE NUMBER 301-227-5887

20130115138

14. ABSTRACT (continued)

and predict the whipping response fared poorly, indicating that this complex phenomenon requires additional study and more complex simulation tools.

CONTENTS

FIGURES

TABLES

INTERNATIONAL SYSTEM OF UNITS (SI) CONVERSION LIST

U.S. CUSTOMARY	METRIC EQUIVALENT
1 inch (in)	25.4 millimeter (mm), 0.0254 meter (m)
1 foot (ft)	0.3048 meter (m)
1 pound-mass (lbm)	0.4536 kilograms (kg)
1 pound-force (lbf)	4.448 Newtons (N)
1 foot-pound-force (ft-lbf)	1.3558 Newton-meters (N-m)
1 foot per second (ft/s)	0.3048 meter per second (m/s)
1 knot (kt)	1.6878 feet per second (ft/s) 0.5144 meter per second (m/s)
1 horsepower (hp)	0.7457 kilowatts (kW)
1 long ton (LT)	1.016 tonnes 1.016 metric tons 1016 kilograms (kg) 2240 pounds
1 inch water (60F)	248.8 Pascals (Pa)

ABSTRACT

The Joint High Speed Sealift (JHSS) segmented model (Model 5663) tests performed in 2007 at Naval Surface Warfare Center, Carderock Division (NSWCCD) were designed to provide a large data set for validation of numerical simulations. The segmented model had a scaled longitudinal stiffness in bending and torsion provided by an aluminum backspline. The hull of the model was cut into segments to lessen the stiffness effects of the shell. The model was self-propelled and steered during data collection. Preliminary validation work performed soon after the experiments with LAMP (Large Amplitude Motions Program) and Numerical Flow Analysis (NFA) showed favorable results. Additionally, the segmented model provided structural loading results that were used to understand hydroelastic phenomena such as springing and whipping. A study of the irregular seas cases showed that springing does not have a large effect on the JHSS model. The whipping response was explored for regular seas runs, with some cases showing significant loads on the ship. Efforts to understand and predict the whipping response fared poorly, indicating that this complex phenomenon requires additional study and more complex simulation tools.

ACKNOWLEDGEMENTS

The authors would like to acknowledge Art Reed, Ph.D., for his insightful discussions and guidance during the planning and preparation of the paper. The authors would like to thank Scott Graham for performing the Orca 3D calculations for the NFA simulations. NFA predictions are supported in part by a grant of computer time from the Department of Defense High Performance Computing Modernization Program (HPCMP). NFA simulations have been performed on the Cray XT4 at the U.S. Army Engineering Research and Development Center.

ADMINISTRATIVE INFORMATION

The work described in this report was performed by the Structures and Composites Division (Code 65) and the Science and Technology Branch of the Resistance and Propulsion Division (Code 583) of the Hydromechanics Department at the Naval Surface Warfare Center, Carderock Division (NSWCCD). The work was performed under work request N0001411WX21557 and work unit numbers 11-1-5800-390-10.

INTRODUCTION

The JHSS model, NSWCCD Model 5663, is a segmented structural model that was built and tested in 2007 in the Maneuvering and Seakeeping Basin (MASK) at NSWCCD in West Bethesda, MD. A segmented structural model is a ship model that has scaled longitudinal bending and torsional stiffness. The scaled stiffness is obtained by building a backspline into the model that accounts for the bending stiffness and segmenting it to isolate the stiffness to the backspline. An alternate way to obtain structural loads would be to build a model with scaled plates and stiffeners; however, this would be very difficult and expensive to build. The backspline allows the stiffness to be scaled properly while using reasonable materials and simple construction.

The purpose of the JHSS Structural Seakeeping Loads tests was to provide an expansive data set of structural loads for validation of numerical tools. The test matrix spans a wide set of wave conditions, including regular and irregular seas, heading angles and speeds, with Froude numbers ranging from 0 to 0.43. This test matrix, which includes about 2000 runs, allows for validation of codes from still water through operational conditions and extreme load conditions.

The data analysis performed for the JHSS model experiments has not been extensive to date. Different aspects of the data have been studied, but much is left to be considered. One aspect of

the model tests that has not previously been considered in detail is the hydroelastic response of the vessel. A segmented model provides a valuable means of studying hydroelastic response. The determination of the vibrational characteristics of the model is important for this study, and the main phenomena of interest are springing and whipping.

JHSS SEGMENTED MONOHULL MODEL (MODEL 5663)

The JHSS segmented monohull model has a length between perpendiculars (LBP) of 20 feet and is 1:47.5255-scale to the full scale ship. More model characteristics are shown in Table 1, and further details can be found in the quick-look report by Devine, et. al., [1]. The segmented model uses an aluminum back spline spanning station 2 to station 18 that scales the structural properties of the full scale ship for vertical and lateral primary bending and torsion. The back spline is outfitted with strain gauges at the breaks between segments to gather structural load data. The shell of the model is split at stations 4, 7, 10, 13, and 16, as shown in Figure 1. The shell segments are connected with 0.006 inch thick sheet latex and sealed with silicone to minimize transmission of forces along the cuts.

Table 1. JHSS Model 5663 characteristics.

Model Property	1:47.5255 Scale Value
LOA	260.04 in.
LBP	240. 00 in.
B_{max}	26.496 in.
D_{mid}	19.392 in.
T_{DWL}	7.091 in.
Displacement	711.4 lbs.
k_{yy} (pitch)	60.15 in.

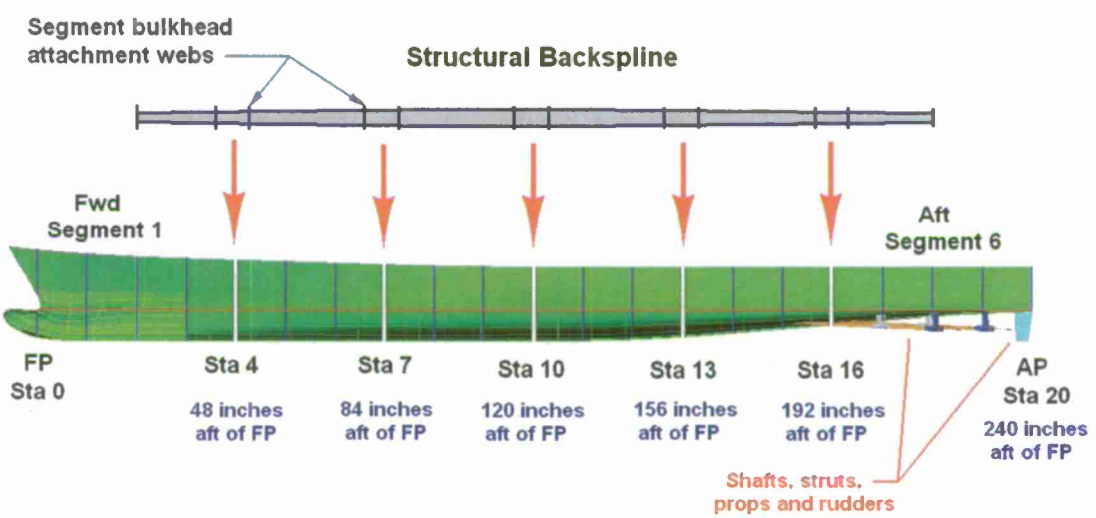

Figure 1. JHSS segmented model (Model 5663) structural layout.

The back spline is attached to the hull segments by bulkheads four inches on either side of the cuts in the shell. The bulkheads are epoxy bonded to the shell and then the back spline is bolted to the bulkheads via flexible tabs on the bulkheads and brackets attached to the back spline. Figure 2 shows the back spline with its brackets and the attachment of the back spline to a pair of bulkheads.

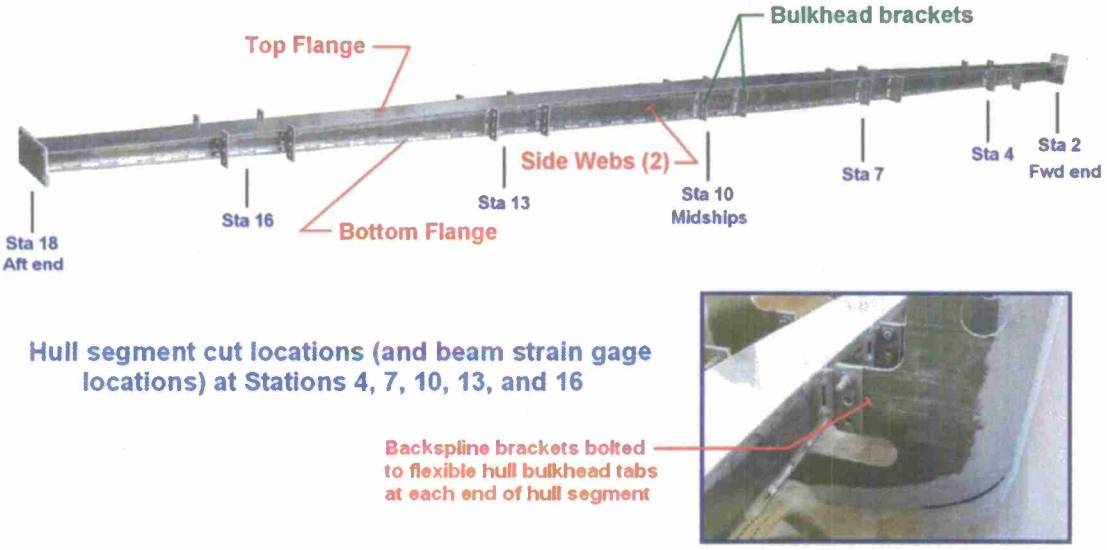

Figure 2. Back spline attachment details.

Secondary loads on the hull are measured using pressure sensors and "slam grillages". The slam grillages consist of arrays of PVC panels outfitted with strain gauges. The panels model the stiffness of the full scale ship shell plating and record the average pressure over each panel during the tests. Two 3x3 arrays are placed on the port side of the hull in Segment 1 to measure wave impacts on the bow. Four more arrays – 2x2 on the starboard side and 4x4 on the port side – are placed on the front of the nominal deckhouse and on the deck directly in front of the deckhouse. The placement is shown in Figure 3. Additionally, four single slam panels are also placed on the hull near the waterline in Segments 2 and 3.

The model is self-propelled by a 3.1 hp electric motor attached to the top of the back spline between stations 10 and 13 (in Segment 4). The motor simultaneously drives four propellers to propel the model, as seen in Figure 4. The drive shafts and gear boxes are mounted in such a way as to minimize vibration and bending moments in the beam transmitted from the drive shafts. The model is steered by two rudders controlled by an operator on the carriage.

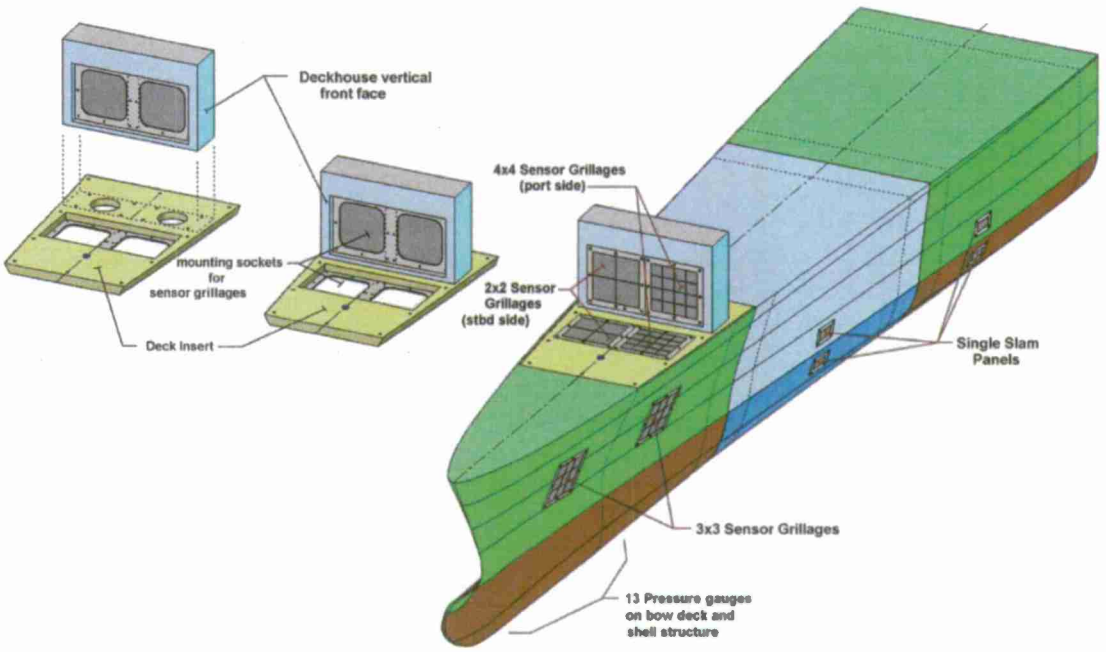

Figure 3. Slam grillage locations.

Figure 4. View of propellers and rudders.

JHSS MODEL 5663 SEAKEEPING LOADS TESTS

Seakeeping loads tests on the JHSS Model 5663 were performed in July and August of 2007 in the Maneuvering and Seakeeping (MASK) Basin at NSWCCD, West Bethesda. Approximately 2000 individual test runs were performed spanning a large test matrix, shown in

Table 2. Data was collected on 118 channels at three different sampling rates. During testing, 43 channels were sampled at 200 Hz, including structural loads (bending moment, torsion, and shear force), motions sensors, wave probes, and propulsion sensors. The slam grillages provided data on 62 channels at 15 kHz and the 13 pressures sensors were sampled at 40 kHz. High sampling rates were used to capture fast, transient events such as wave impact.

In addition to the raw data collected, four video cameras captured the test runs at 30 frames per second. The four cameras were placed at the port stern, port bow, forward of the bow, and on the deckhouse. The video allows for insight into the nature of the runs years later that the data alone cannot give. Example frames from Camera 2 (Port Bow) for run 478 (15 knots, 1/15 regular waves, head seas) are show in Figure 5 and Figure 6. For the seakeeping runs, both with regular and irregular waves, the wave makers were started while the model was stationary. The model was accelerated by the carriage via bow and stern tow lines to get it up to speed. The propulsion motors were then activated and the data acquisition equipment started. The model was self-propelled and steered while all data was collected.

Figure 5. Run 478 bow impact event and extreme sagging moment.

Figure 6. Run 478 deck house impact and extreme hogging moment.

Table 2. JHSS seakeeping loads test matrix.

Irregular Waves

Speed (knots)	Sea State 5 (SS5)	Sea State 6 (SS6)	Sea State 7 (SS7)	Sea State 8 (SS8)	Hurricane Camille
0	180°	180°, 270°	180°, 270°	180°	-
5	-	-	-	-	180°
15	180°, 210°, 225°, 270°, 315°, 0°	180°, 225°, 270°, 315°, 0°	180°, 225°, 270°, 315°, 0°	180°, 210°, 225°, 270°, 315°, 0°	180°, 210°, 225°, 270°, 315°, 0°
25	180°, 210°, 225°, 270°, 315°, 0°	180°, 225°, 270°, 315°, 0°	180°, 210°, 225°, 270°, 315°, 0°	180°, 210°, 225°, 270°, 315°, 0°	-
35	180°, 210°, 225°, 270°, 315°, 0°	180°, 210°, 225°, 270°, 315°, 0°	180°, 210°, 225°, 270°, 315°, 0°	180°, 225°, 270°	-
45	180°, 210°, 225°, 270°, 315°, 0°	180°, 210°, 225°, 270°, 315°, 0°	180°, 210°, 225°, 270°, 315°, 0°	180°, 225°, 270°	-

Regular Waves

Wave slope	Speed (knots)	180° Heading	210° Heading
1/50	15	x	x
	25	x	x
	35	x	x
	45	x	x
1/30	15	x	x
	25	x	x
	35	x	x
1/15	5	x	
	15	x	

Notes:

1. Regarding headings:
   180° is head seas, 210° is bow seas, 225° is bow quartering seas, 270° is beam seas, 315° is stern quartering seas, and 0° is following seas
2. For each combination of heading, speed, sea state and wave type, target was minimum cumulative 30 minutes full-scale (261 seconds model-scale) or 20 runs.
3. Runs were rejected due to towing tugs or poor model steering control.
4. In addition, roll decay and calm water spead tests were conducted at speeds of 0, 5, 15, 25, 35, and 45 knots.
5. Approximately 2000 total test runs were completed.

NUMERICAL SIMULATION COMPARISON

LAMP-2

The main purpose of the JHSS Segmented Model Tests was to provide data for validation of numerical simulations. The Large Amplitude Motion Program (LAMP) for non-linear seakeeping was the first simulation to be compared to the experimental data. The validation between LAMP and the experiments was performed by Code 654 using the motions and structural force data. The version of LAMP used was LAMP-2, which uses approximate body non-linear theory. Figure 7 through Figure 10 show the comparison of the LAMP predictions with model measurements. The comparisons are good; however, LAMP-2 tends to under-predict the vertical bending moment.

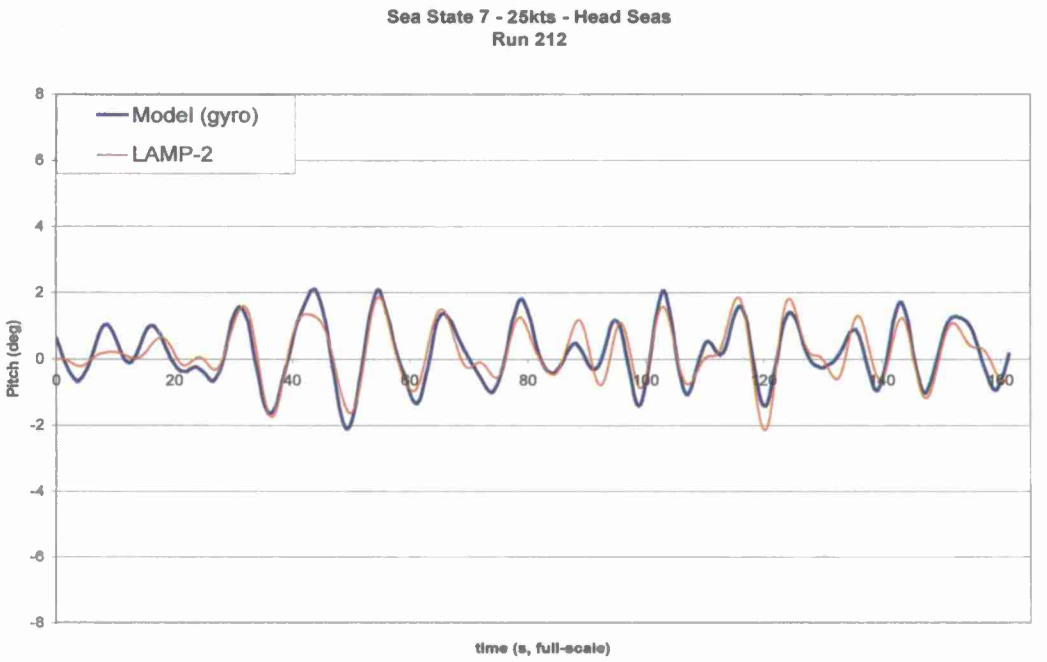

Figure 7. Pitch angle comparison of LAMP-2 simulation with model measurements for SS7 head seas at 25 knots [2].

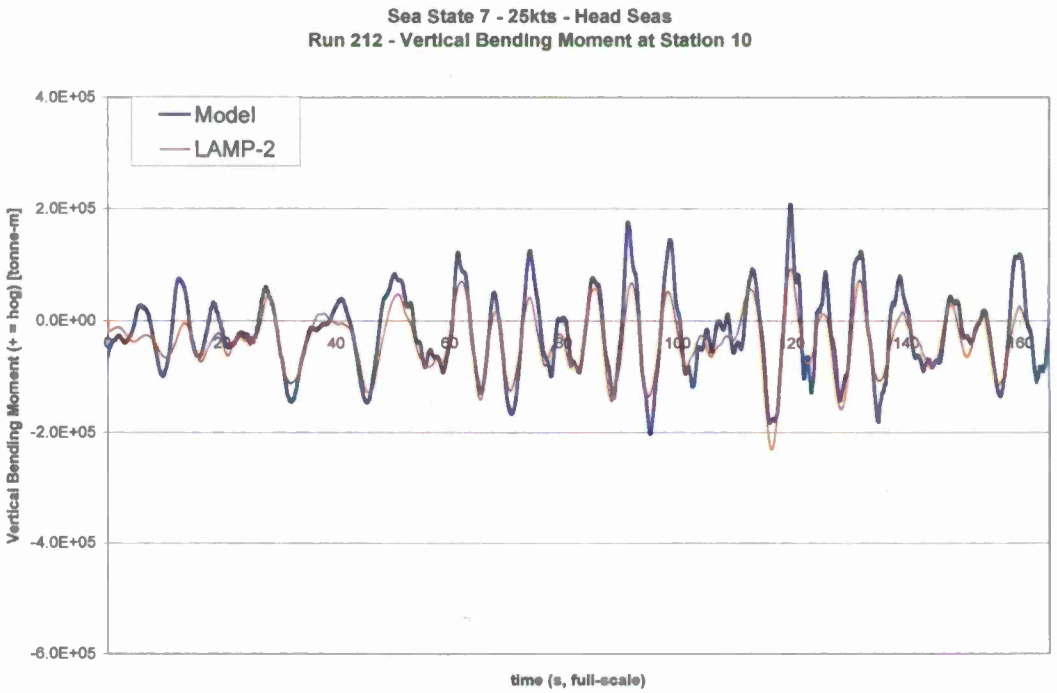

Figure 8. Vertical bending moment comparison of LAMP-2 simulation with model measurements for SS7 head seas at 25 knots [2].

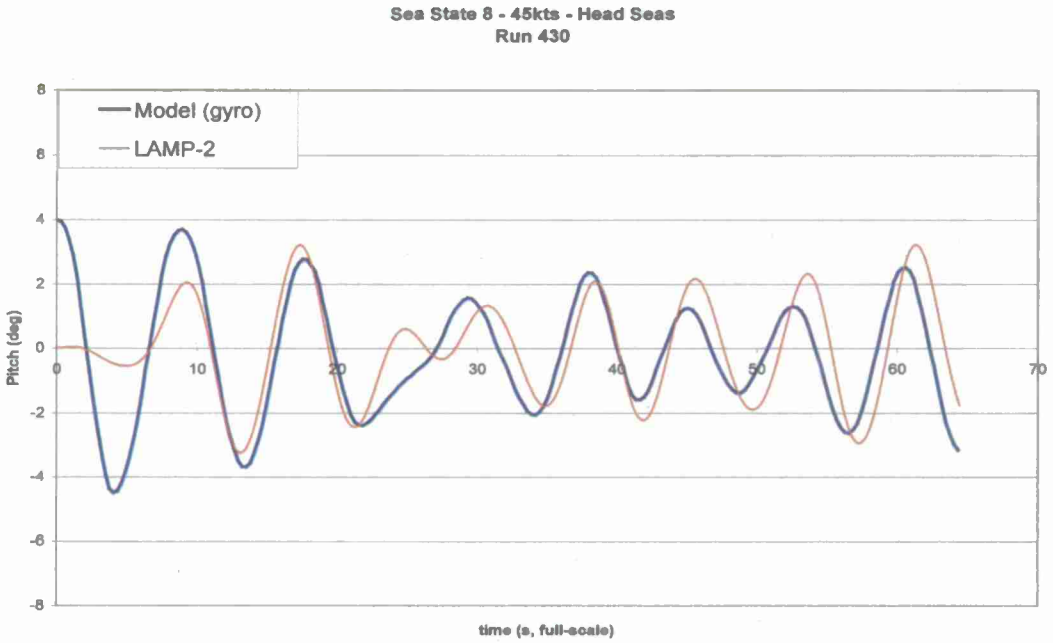

Figure 9. Pitch angle comparison of LAMP-2 simulation with model measurements for SS8 head seas at 45 knots [2].

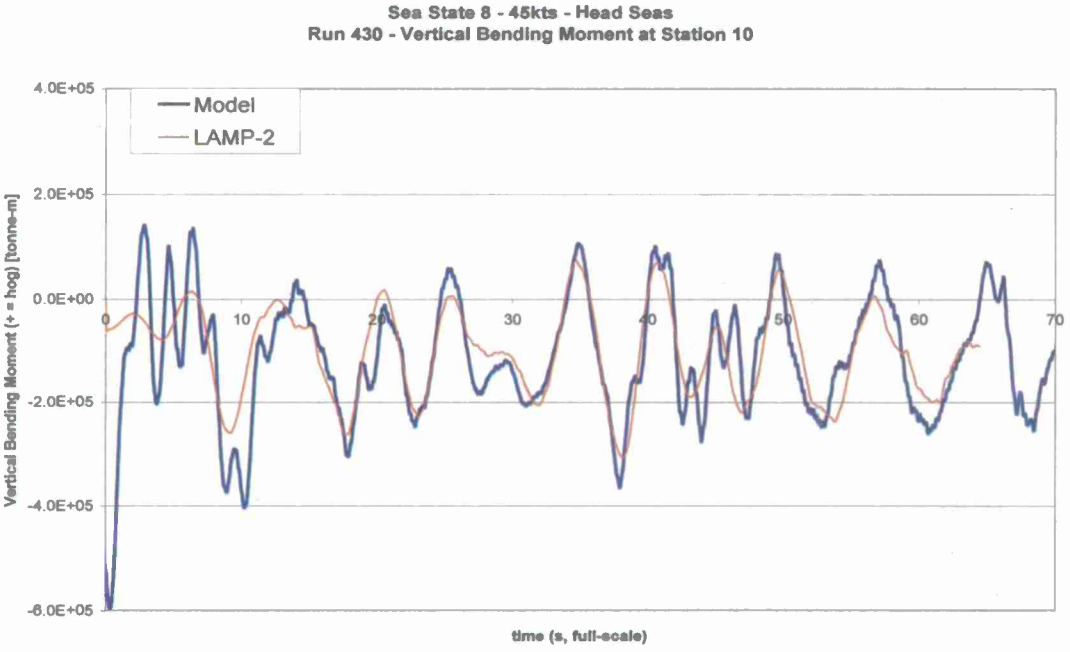

Figure 10. Bending moment comparison of LAMP-2 simulation with model measurements for SS8 head seas at 45 knots [2].

NFA

Simulations also were performed using SAIC's computational fluid dynamics (CFD) tool Numerical Flow Analysis (NFA). NFA approximates a solution to the Navier-Stokes equations utilizing a cut-cell, Cartesian-grid formulation with interface-capturing to model the unsteady flow of air and water around moving bodies. The interface-capturing of the free surface uses a second-order accurate, volume-of-fluid technique. The cut-cell method is used to enforce free-slip boundary conditions on the body. NFA uses an implicit subgrid-scale model that is built into the treatment of the convective terms in the momentum equations [3]. A panelized surface representation of the ship hull (body) is all that is required as input in terms of body geometry. The numerical scheme is implemented on parallel computers using Fortran 90 and Message Passing Interface (MPI). The interested reader is referred to [4], [5], and [6] for a detailed description of the numerical algorithm and of its implementation on distributed memory High Performance Computing (HPC) platforms.

The numerical simulations are normalized by the model ship length (L = 240.0 inches) and the ship speed (U =4.78 kts), corresponding to a Froude Number, of Fr =$U/\sqrt{(gL)}$ =0.31, which corresponds to a full-scale speed of 30 knots. It is noted that in the simulations in which the model is free to move, no roll stabilization mechanisms, such as bilge keels are present. In all the simulations, the bow of the ship is fixed at x=0 and the flow is from positive x. Inflow and outflow boundary conditions are used in the stream-wise direction, and free-slip conditions are used in the cross-stream and vertical directions. The inflow condition is either a free-stream current or waves based on second order Stokes wave theory.

The extents of the computational domain in the stream-wise (x), span-wise (y), and cross-tream (z) directions are respectively [1.5L, -4L], [-2L, 2L], and [-1.25L, 0.75L]. Three computational domains and time steps are employed and are herein referred to as coarse (c) medium (m), and fine (f). The number of gridpoints [nx, ny, nz] are $[512, 256, 128]^c$, $[1024, 512, 256]^m$, and $[2048, 1024, 512]^f$. The time steps for the coarse, medium, and fine simulations are respectively Δt=0.002, 0.001, and 0.0005. The grid points are distributed in 128x64x64 blocks over 32 and 256 cores for the coarse and medium simulations, respectively. In the fine simulation, the grid points are distributed in 128x128x64 blocks over 1024 cores. The grid is stretched with nearly uniform spacing around the ship where the grid spacing is $0.008L^c$, $0.004L^m$, $0.002L^f$. The maximum grid spacing far away from the ship along the Cartesian axes is $[0.028L, 0.073L, 0.112L]^c$, $[0.014L, 0.037L, 0.056L]^m$, $[0.006L, 0.018L, 0.028L]^f$.

All simulations have been run on the Cray® (Cray Inc.) XT4 at the U.S. Army Engineering Research and Development Center (ERDC). The coarse simulations require one hour per boat length. The medium simulations require 2.2 hours per boat length. The fine simulations require nine hours per boat length. The forces and moments are output every two iterations for all cases. This data output rate corresponds to a dimensional sampling frequency of 200Hz, 400Hz, and 800Hz for the coarse, medium and fine grids, respectively.

Static Stability

The results of a hydrostatic stability analysis of the JHSS model are presented to provide a baseline to which the stability at forward speed and in waves can be compared. Figure 11 shows the cross-section of the JHSS model at mid-ship, the water static water line (horizontal blue line), with the positions of the center of gravity (G), center of buoyancy (B), keel depth (K), and meta-centric height (M), drawn to scale. The meta-centric height, M, is calculated as:

$$\overline{GM} = \overline{KB} + \overline{BM} - \overline{KG} \quad (1)$$

Based on linear theory $\overline{BM}$ may be estimated as:

$$\overline{BM} = \frac{I_{xx}}{\nabla} \tag{2}$$

where I_{xx} = moment of inertia of the waterplane area
and ∇ = volume of water displaced by the boat.

The center of buoyancy, B, and the moment of inertia of the water plane, I_{xx}, are computed by slicing the panelized geometry into thin strips in z and computing the appropriate contour integrals for the moments of inertia and area. These quantities are computed to check the static righting curve, as the total righting moment about the x-axis and displacement are directly output from NFA. Hence the righting arm can be directly calculated as:

$$\overline{GZ} = \frac{R_m}{\Delta} \tag{3}$$

where R_m = total moment about the x axis
and Δ = displacement

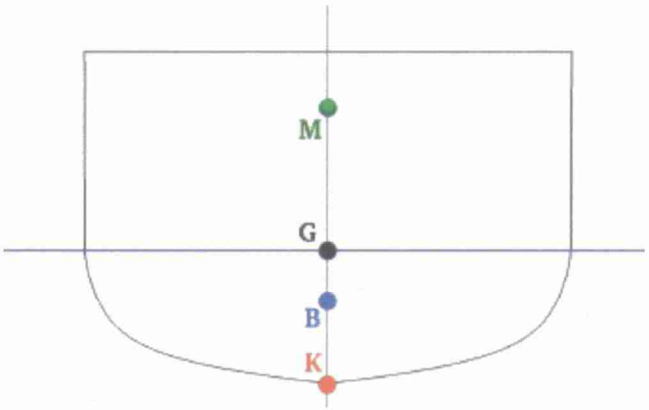

Figure 11. The cross-section of the JHSS model at midship with the hydrostatic waterline (horizontal blue line). Also shown are the positions of the center of gravity, G, center of buoyancy, B, keel depth, K, and meta-centric height, M.

The hydrostatic righting arm curve in Figure 12 is created by rolling the model in small angular increments and then iteratively sinking and trimming the rotated model until it is in hydrostatic equilibrium. This hydrostatically balanced, rotated, sunk and trimmed model is used as the input for the steady forward speed and head seas studies. Figure 12 shows the hydrostatic stability curves and the approximations $\overline{GM}\phi$ and $\overline{GM}\sin\phi$. The results are shown for various vertical centers of gravity (VCG), as the 4DOF simulation uses a more unstable VCG position. All other simulations use VCG=0, i.e., at the static water line.

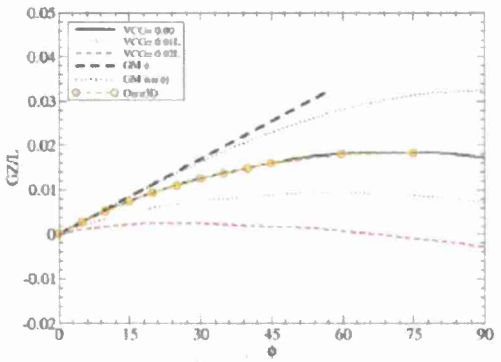

Figure 12. Righting arm as a function of heel angle. Also shown in red are the changes with respect to the position of the vertical center of gravity (VCG).

Effect of Steady Forward Speed

The effect of steady forward speed on the righting arm is considered for a heel angle of 30°. Figure 13 serves a dual purpose; the first is to illustrate that the solution converges as the grid is refined, and the second is to show the correction to the righting moment that occurs when the unsteady two-phase flow around the hull is included. The coarse (black), medium (red), and fine (blue) results are shown in addition to the hydrostatic righting arm (dashed black line). Between T=0 and T=2, the flow is accelerated from rest to the free-stream value. After the initial transient, the righting arm increases to 0.01266L, a 1.6% gain over the hydrostatic value.

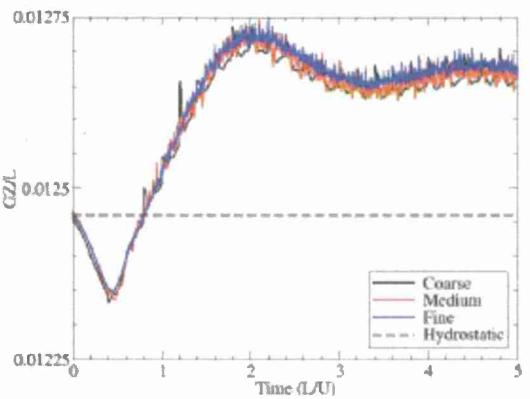

Figure 13. The effect of steady forward speed on the righting arm at 30° heel. The grid resolutions and time steps corresponding to coarse, medium, and fine results are given in the Numerical Approach section.

Stability in Waves

All simulations that are discussed hereafter are in waves. The wavelength, λ, is equal to the ship length ($\lambda = L$), and the amplitude, a, of the waves is $a = 0.015L$. The waves are specified over a region of $0.5L$ at the front of the domain based on second-order Stokes wave theory [7]. The waves then travel towards the ship where the full interaction of the ship and waves is simulated. The NFA results include the effects of wave radiation and diffraction. To quantify the effects of wave radiation and diffraction, a simulation of the waves with no body is performed and the resulting pressure field is used to calculate the Froude-Krylov force on the body. The results of an NFA simulation of the JHSS monohull at a fixed heel angle of 30° in waves with

$\lambda = L$ and $a = 0.015L$ at the medium grid resolution are shown in Figure 14, Figure 15, and Figure 16. Figure 14 compares the hydrostatic righting arm calculated based on the Froude-Krylov force to the righting arm from NFA. In the subsequent discussion, the wave phase, θ, is as follows: zero phase is defined as the phase when the crest of the wave is at the bow. Comparing the positive and negative changes to the righting arm in Figure 14, the Froude-Krylov prediction is in better agreement for gains to the righting arm (θ =0°-30°,180°-360°), albeit with a phase-lead. Losses to the righting arm are over-predicted. The maximum over-prediction is 7% and occurs at θ =130°. Figure 15 shows the waves when (a) the maximum loss in righting arm occurs, (b) the righting arm is equal to the hydrostatic righting arm, and (c) the maximum gain in righting arm. Figure 16 shows the stacked data from six full wave periods (open circles) plotted along with the average over all six wave periods (solid black line). The six wave periods were all after T=2 when fully developed waves were along the entire length of the boat. The phase average is in good agreement with the instantaneous values.

The results of NFA simulations at heel angles of 10°, 20°, 30°, 40°, 50°, and 60° with the same waves and at the medium grid resolution are used to construct figures similar to Figure 16. These plots are used to construct Figure 17, which shows the change in righting arm as a function of heel angle, for lines of constant wave phase. The maximum righting arm lost, -10%, occurs at a heel angle of 60° and phase angle of 120°. The maximum righting arm gained, +10%, occurs at a heel angle of 60° and phase angle of 300°.

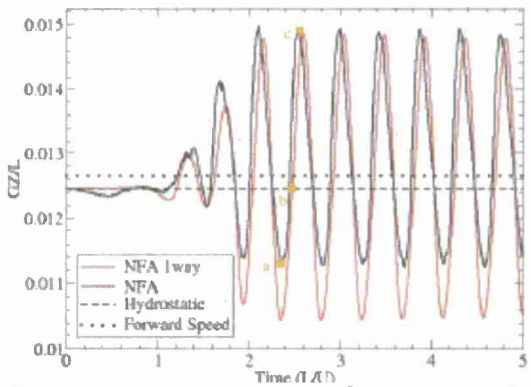

Figure 14. Comparison of righting arms as a function of wave phase (time) for 30° heel. The two-way coupled NFA predictions are shown in black. The one-way couple NFA predictions based on a Froude-Krylov force are shown in red. The points labeled a, b and c correspond to the waves shown in Figure 15.

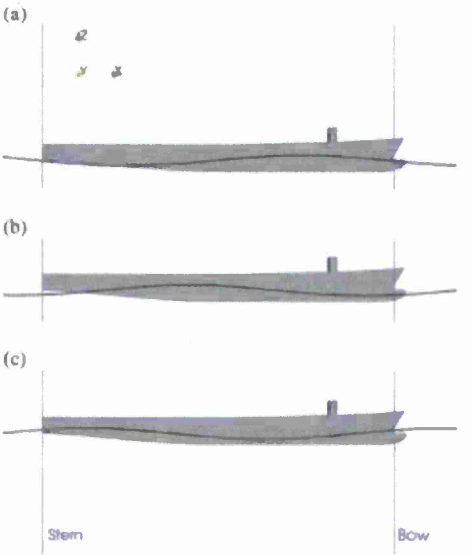

Figure 15. Position of waves when (a) maximum loss to righting arm, (b) no loss or gain to righting arm, (c) maximum gain to righting arm.

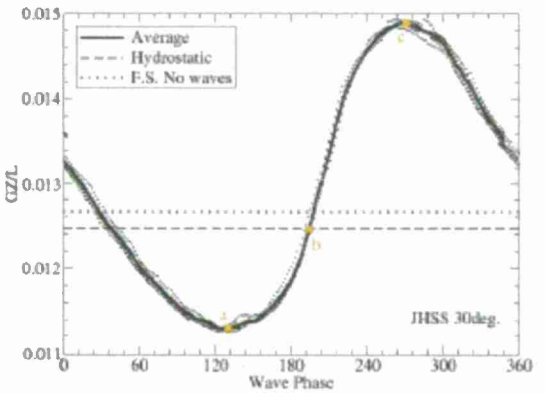

Figure 16. The effect of waves on the righting arm at 30° heel. Data (shown as open circles) is from six wave periods. The solid black line is the average, the dashed black line is the hydrostatic righting arm, and the dotted black line is the righting arm at steady forward speed. The points labeled a, b and c correspond to the waves shown in Figure 15.

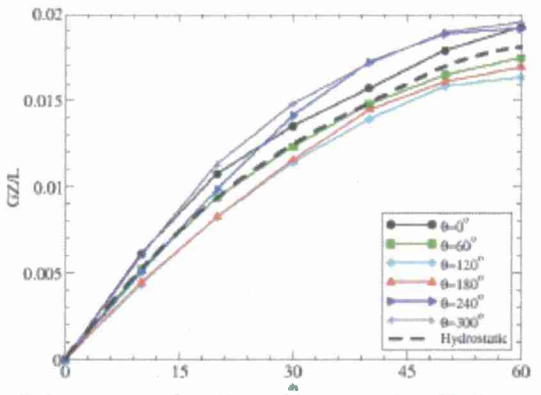

Figure 17. Change in righting arm as a function of heel angle with lines of constant wave phase. The hydrostatic righting arm curve (- - -) is plotted for comparison.

Attention is now focused on the results of a 4DOF simulation. The JHSS monohull model at 0° initial heel is put in waves and free to sway, heave, roll, and pitch. Without propulsion and rudders, surge and yaw would allow the model to be pushed parallel to the waves and exit out of the domain, and hence both are fixed at zero for the simulations. Based on the hydrostatic stability plot, the vertical position of the center of gravity (VCG=0.025L above the mean water line) was chosen so that roll of more than ~30° should allow for capsizing only when additional losses to the righting arm due to wave interactions occur. Figure 18 shows a time series of renderings from the 4DOF simulation illustrating the capsizing in head seas.

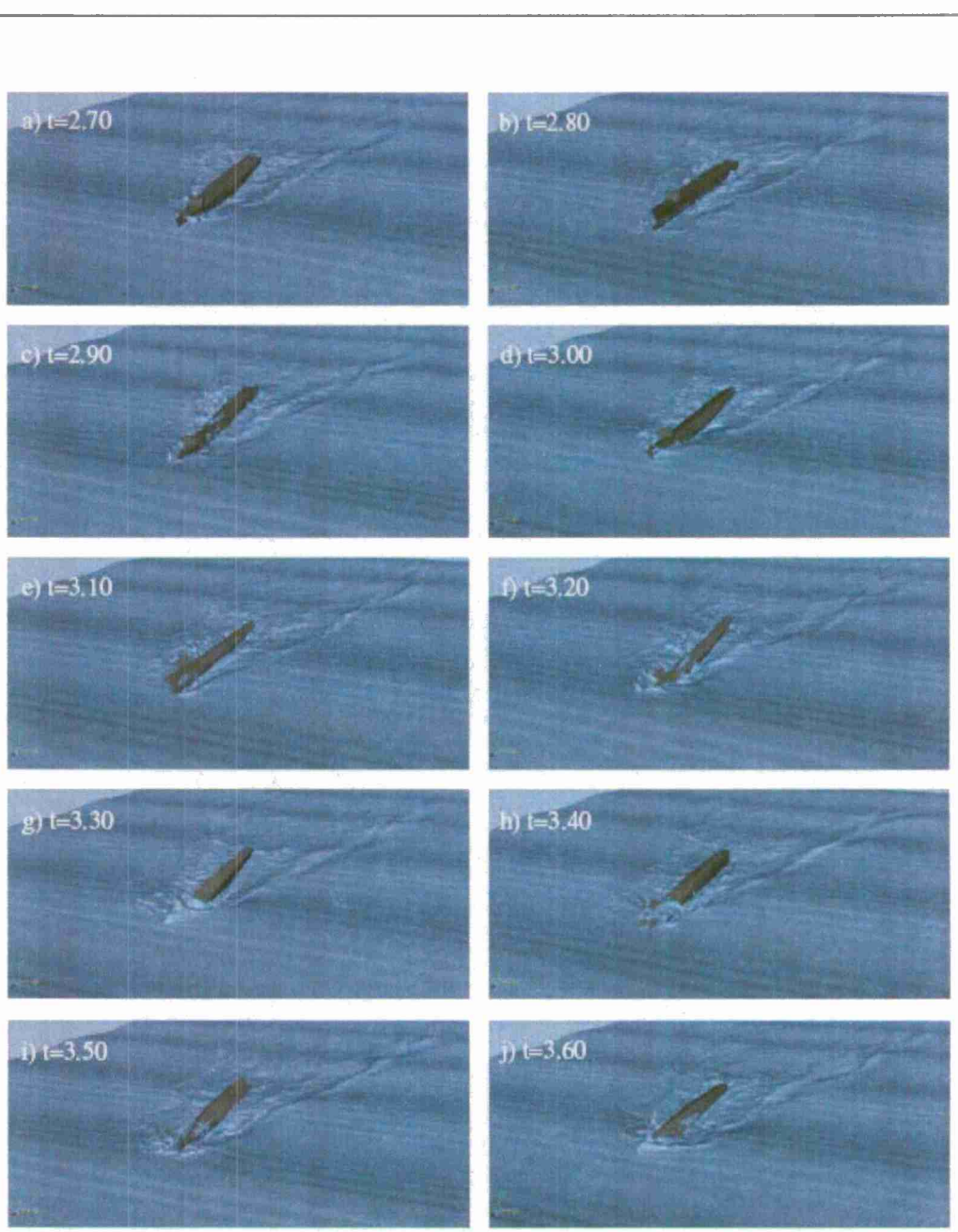

Figure 18. Instantaneous visualizations of a 4 DOF simulation of the JHSS monohull in head-seas with a = 0.015L and l = L, where L is the ship length, l is the wave length, and a is the wave amplitude.

DATA ANALYSIS OF STRUCTURAL RESPONSE

Natural Frequency and Mode Shape Estimation

The natural frequencies of the JHSS monohull model are used to understand the hydroelastic response of the vessel, as explained in the following two sections. The stiffness and mass distributions are estimated using information measured from the model before the experiments. The shell is assumed to not contribute to the stiffness of the model, thus the

stiffness is assumed to be completely provided by the backspline. The moments of inertia of the aluminum backspline are calculated from the built up sections at each station, as shown in Table 3. For the values in the table, the local x-axis is the port-starboard axis, and the y-axis is the vertical axis (the structural convention for beams, not the convention for a ship coordinate system.) The inertias at the ends of the ship (Stations 0 and 20) are estimated by linearly extrapolating from the end of the backspline.

Table 3. Structural moments of inertia of JHSS model backspline.

Station	I_{xx} [in^4]	I_{yy} [in^4]
2	1.61897	2.54681
3	2.24072	3.05525
4	3.02666	3.69607
5	3.97674	4.91360
6	5.26540	7.07229
7	6.70391	9.68738
8	8.00817	12.12133
9	8.96446	13.97371
10	9.37592	14.90366
11	9.10871	14.70449
12	8.26511	13.70549
13	7.01453	12.37013
14	5.56620	11.10607
15	4.27292	10.09866
16	3.39809	9.42385
17	2.78980	8.94219
18	2.44810	8.66793

The mass of the model is recorded in terms of the masses and centers of the six segments. For the natural frequency analysis, a linearly varying distributed mass is applied to each segment that matches the mass and center of mass for that segment. The distribution is described by the mass per unit length values at the endpoints of the segments. The mass distribution is summarized in Table 4.

Table 4. Mass properties of JHSS segments.

Segment	Weight [lb]	x_{cg} [ft aft FP]	m_1 [slug/ft]	m_2 [slug/ft]
1	88.705	2.360	0.0269	0.0900
2	129.564	5.524	0.1083	0.1192
3	138.417	8.818	0.0442	0.1988
4	139.833	11.698	0.0742	0.1714
5	103.292	14.519	0.0872	0.0941
6	99.167	18.037	0.0617	0.0689

Drawings for the model are used to approximate the shape of the hull to estimate hydrostatic and hydrodynamic properties. The hydrostatic properties provide a distributed stiffness in the vertical direction from the change in buoyancy. The hydrodynamic added mass is approximated using Lewis forms (a series of ship-like sections [8]) to provide sectional added mass coefficients. Lewis forms are defined for a range of local beam to draft ratios and section shapes. The two-dimensional added mass coefficients give added mass per unit length for the

model when dimensionalized. The added mass values at the ends of the segments are supplied in Table 5.

Table 5. Sectional added mass of JHSS model.

Station	0	4	7	10	13	16	20
a33 [slugs/ft]	0.0000	0.6406	2.1291	4.0862	4.0862	3.5295	1.5367

The model is discretized into finite elements to obtain the natural frequencies. The ends of the segments are used as the nodes because that is where the mass information is known about the model. The finite elements assume linear distributions of bending stiffness and distributed mass to generate local element stiffness and mass matrices. These local matrices are assembled into four global matrices – bending stiffness [K], hydrostatic stiffness [C], model mass [M], and hydrodynamic added mass [A]. The matrices are used to determine the natural frequencies and mode shapes of the structure by solving the eigenvalue problem shown in Equation (4):

$$([K] + [C])\vec{v} = \omega^2([M] + [A])\vec{v} \tag{4}$$

The natural frequencies obtained from the equation above do not account for three-dimensional effects. These effects could not be included in the matrix equation of motion because they depend on the mode number. To account for the three-dimensional effects, the modal stiffness (k_n^*), mass (m_n^*), and added mass (a_n^*) were found for each mode shape using Equation (5) for the modal mass, and similar equations for the other quantities. Equation (6) was then applied to correct the natural frequencies. The J_n factor is based on vibrations of an ellipsoid with the same length to beam ratio and different for each mode number n [9] This process does not exactly account for the three-dimensional effects because the mode shapes ($\overrightarrow{v_n}$) are orthogonal with respect to ([M] + [A]), not to [M] and [A] individually, leading to coupling terms between the modes. These coupling terms have been neglected for this analysis because they are small relative to the diagonal terms.

$$m_n^* = \overrightarrow{v_n}^T [M] \overrightarrow{v_n} \tag{5}$$

$$\omega_n^2 = \frac{k_n^*}{m_n^* + J_n a_n^*} \tag{6}$$

The natural frequencies of the model without hydrostatic or hydrodynamic effects were also determined for comparison. These are labeled as the "dry" frequencies, while those with the effects from the water are the "wet" frequencies. The natural frequencies for the first five mode shapes (two rigid body, three elastic) are included in Table 6, converted to Hertz. The second column shows the frequencies before the correction for three-dimensional effects is applied, and the fourth column shows the frequencies after the correction is applied. The first two elastic modes are also shown in Figure 19 using the finite element interpolation functions to show the deflection between nodes. Of note is that the two rigid body modes contain coupled heave and pitch when hydrostatic forces are taken into account, while heave and pitch can be uncoupled without hydrostatics.

Table 6. Estimated natural frequencies of JHSS model.

Mode #	f_n dry [Hz]	f_n wet [Hz]	f_n corrected [Hz]
1	0.0000	0.8333	0.8451
2	0.0000	0.8833	0.8974
3	6.4417	4.0902	4.3624
4	14.553	9.0472	9.8475
5	26.559	16.313	17.922

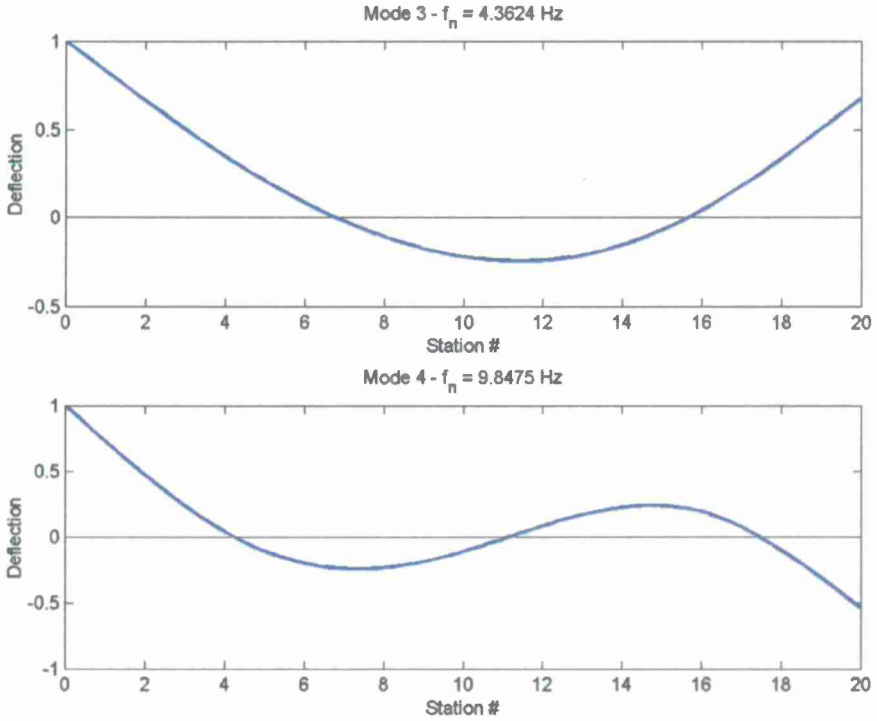

Figure 19. First two vertical bending vibrational mode shapes.

Springing Response

Springing is a resonance phenomenon in which the primary longitudinal bending mode on a ship is excited by continual wave loading from the sea spectrum. The amount of wave energy at the natural frequency of the ship is usually very small compared to lower frequencies, however because the damping is usually small for longitudinal vibrations, the response can be significant. Springing will be most severe for long, slender vessels because of their lower natural frequencies [8]. The severity is also increased for higher speed vessels because the frequency of encounter increases with speed for head seas. This relationship can be seen in Equation 7, where ω_e is the encounter frequency, ω_0 is the wave frequency, U is the speed of the ship, κ is the wave number, and β is the heading angle, with 180° as head seas.

$$\omega_e = \omega_0 - U\kappa \cos\beta \tag{7}$$

The springing response is analyzed by studying the input wave spectra (Z(f)) and bending moment response spectra (BM(f)) from the irregular seas runs. The spectra are generated by ensemble averaging the spectra from all runs for a particular case. The spectra from the individual runs are created using MATLAB's built in Fast Fourier Transform (FFT) algorithm.

To generate smooth spectra, spline curves are fitted to the ensemble averaged spectra. For this analysis, the fitting has been done on the magnitude of the spectra; therefore, the negative portions of the curves are just artifacts of the fitting process.

The JHSS monohull model does not show large springing response at the 45 knot full scale equivalent speed. Examples are shown in Figure 20 and Figure 21, where the response at the first natural frequency of the structure (between 4 and 5 Hz) is small compared to the wave induced response, and is likely due to the wavelength that occurs at the natural frequency of the structure. This wave length is about one-fifth of the length of the ship at 45 knots, as shown in Figure 22, and will only get smaller with a decrease in speed. This small wavelength will not excite the lower modes of vibration due to cancellation effects.

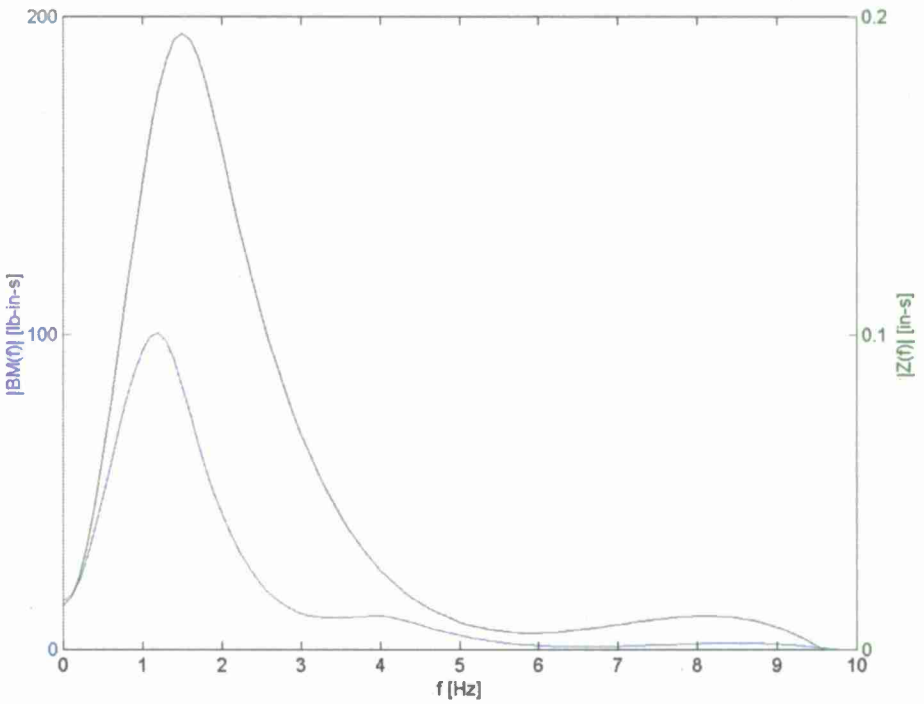

Figure 20. Sea State 5, 45 knot, head seas input (Z(f)) and bending moment response spectra (BM(f)).

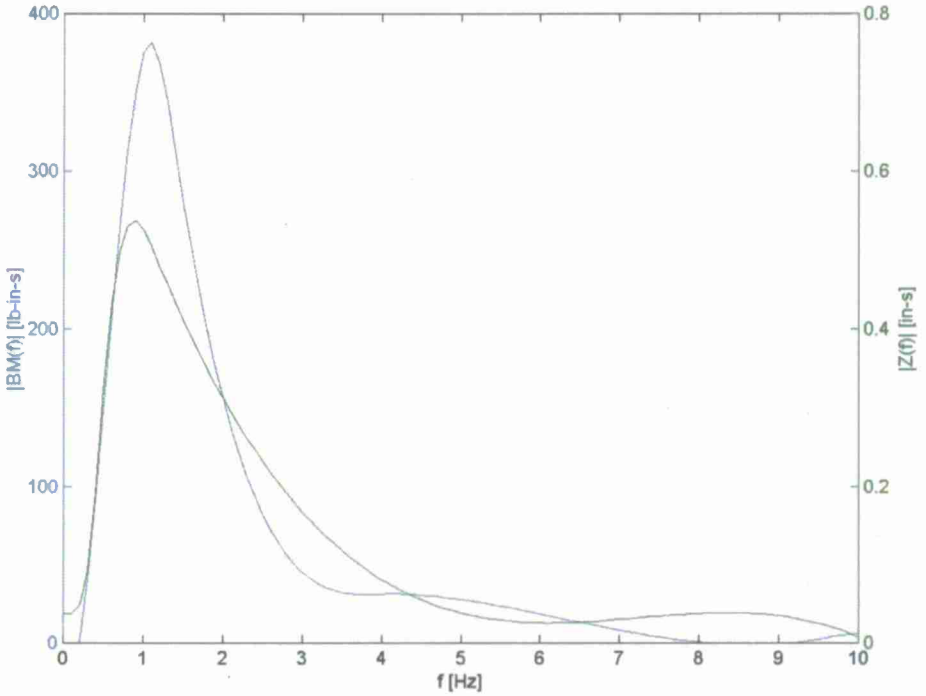

Figure 21. Sea State 7, 45 knots, head seas input (Z(f)) and bending moment response spectra (BM(f)).

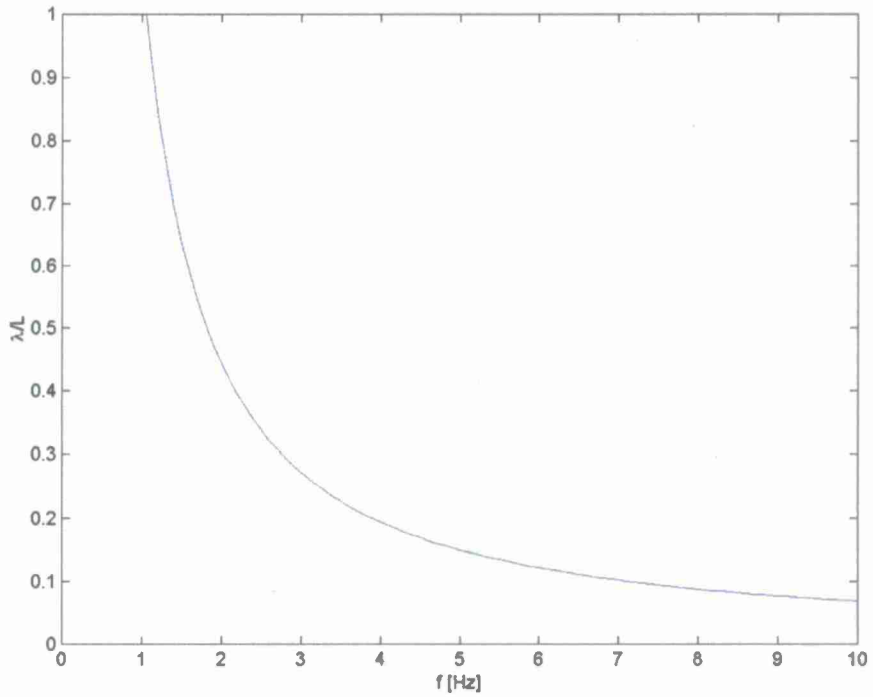

Figure 22. Wavelength versus encounter frequency for 45 knot, head seas cases.

Whipping Response

Whipping is a transient hydroelastic response that is caused by impulsive loads on the ship, such as bow and stern impacts. The impacts result in a "ringing" response in the structure that decays due to damping. The response usually is only significant in the first few mode shapes for vertical bending, especially the first two (2-noded and 3-noded vibration). Whipping is important to study because the phenomenon can cause stresses on the same order of magnitude as the wave induced stress. Unfortunately, the whipping response of a vessel is difficult to predict because of the non-linear and complex nature of the loading. Time domain simulations must be used that accurately account for the free surface position to accurately obtain the response. For design, dynamic amplification factors are often applied to the rigid, quasi-static loading for their simplicity.

The whipping response of the JHSS segmented model is studied using the regular seas runs. The pressure on slam panel G1 is used to determine when the bow of the model impacts the waves. These impact events give an estimate for times to expect an impulsive load and subsequent whipping response of the model. The midship bending moment is then decomposed into low frequency and high frequency components. The low frequency component is the wave induced moment. This wave induced moment is nearly steady state, with the variations from harmonic response similar to the variations in the wave profile. The high frequency component of the bending moment contains the transient bending response of the model. The whipping response is visible in this high frequency response, with events of sharp increase followed by a decaying sinusoid. Figure 23 shows the decomposed bending response and pressure on slam panel G1 for the 15 knot, 1/15 regular wave, head seas case. An important point is that the whipping response for this vessel can be a significant portion of the total response and therefore is important for design load generation.

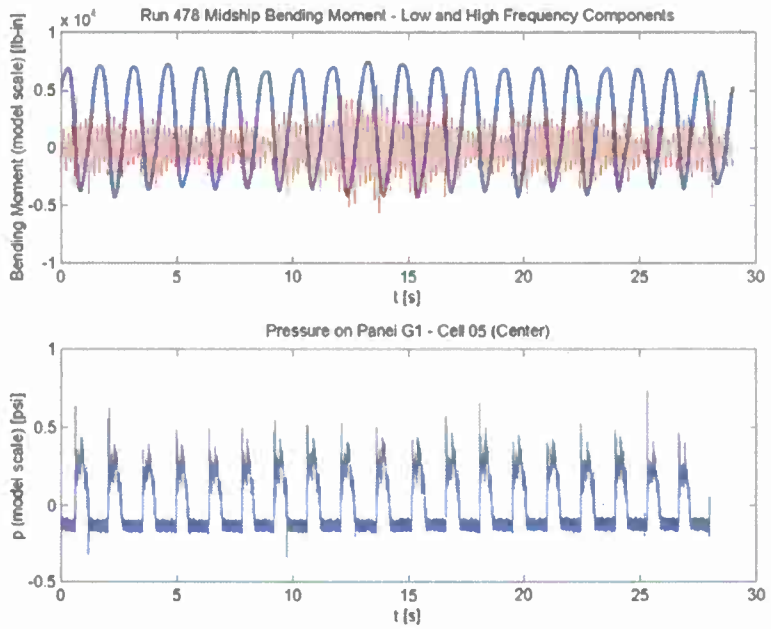

Figure 23. Midship bending moment low and high frequency components (top panel), and pressure at the center of slam panel G1 (bottom panel) for Run 478 (15 knots, 1/15 regular waves, head seas).

The prediction of the whipping response is a difficult problem. As shown in Figure 23, the whipping response can vary greatly when the pressure on the hull (and thus the wave loading) does not vary greatly. This complex response is indicative of a non-linear system. The source of this non-linearity is not intuitively obvious, and thus is the object of study. The deflection remains small throughout the experimental runs, as shown in Figure 24. The maximum deflection at either end is about one inch relative to the center of gravity. The slope associated with this deflection is about $1/120 \approx 0.00833 \approx \text{atan}(1/120)$, which is an assumption for linear beam theory. Therefore, the non-linearity in the response should not be due to non-linear beam bending. The verification of small deflections also points to using modal expansion to simplify simulations of the structural deformation.

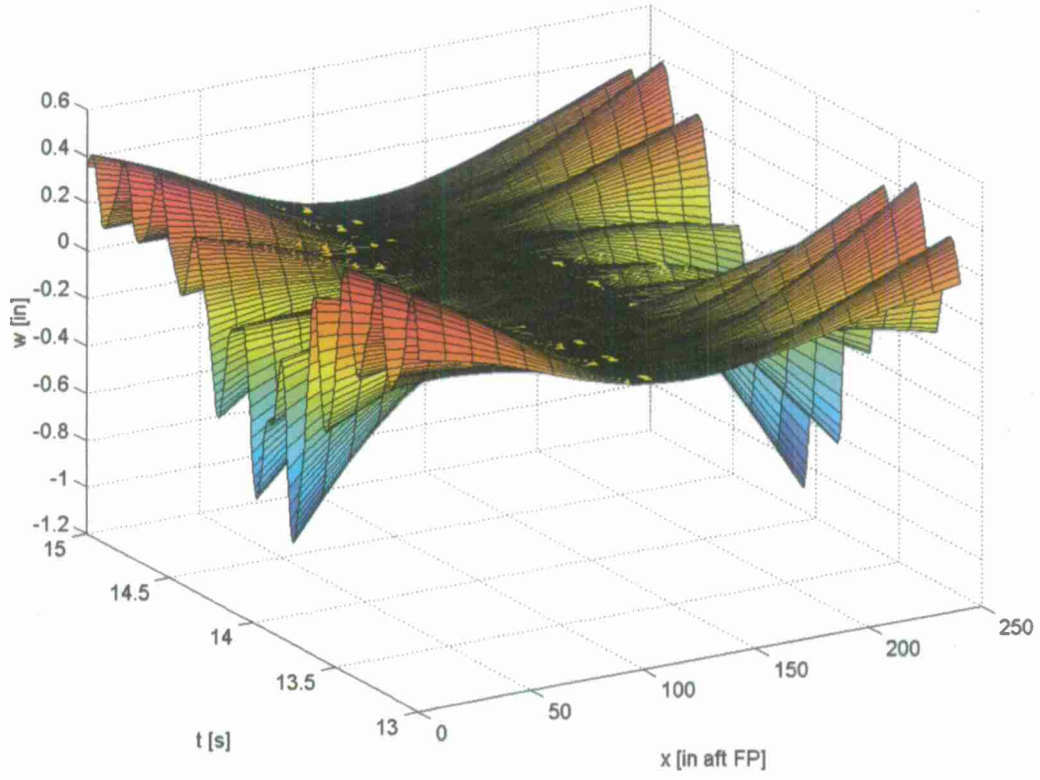

Figure 24. Deflection of JHSS Model for selected period of time – Run 478 (15 knots, 1/15 regular waves, head seas).

The source of the non-linearity in the system can be seen in the response spectrum. The spectrum for Run 478 is shown in Figure 25. The figure shows the first through fourth harmonics of the wave induced excitation, which are also present in the wave spectrum for the run. The response of the model at these frequencies, including the super-harmonics, is consistent with linear theory.

A further expectation for the response spectrum is to have a sharp peak near the first natural frequency in vertical bending. However, the spectrum is spread around the frequency predicted in Section 5, which is about 4.36 Hz. This frequency spreading is not an artifact of the Fast Fourier Transform (FFT) used to generate the spectrum. It is because the frequency of vibration is changing over time due to the changing wetted surface of the ship, which then affects

the hydrodynamic added mass and hydrostatic stiffness. These changes are non-linear in the vessel motions, making them more difficult to predict.

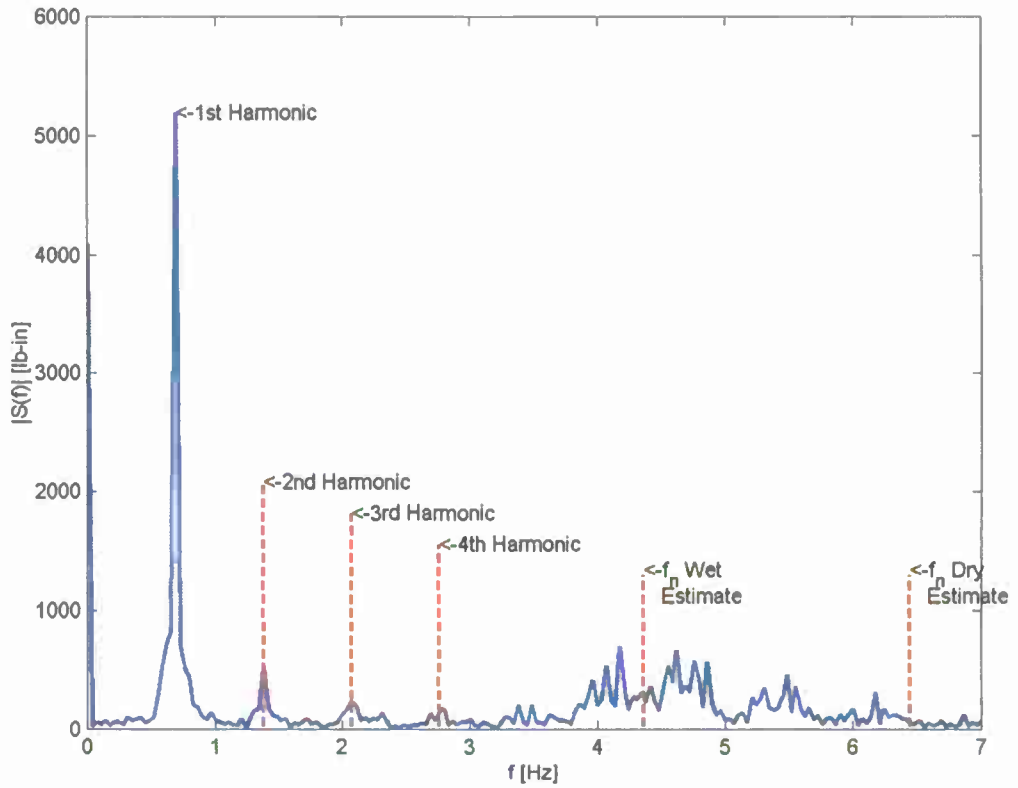

Figure 25. Midship bending moment response spectrum for Run 478.

Simple Model Prediction of Bending Moment

The structural response of the JHSS was then predicted using simple models where the measured rigid body motions (heave and pitch) were used. The waves were reduced to a single frequency component and propagated along the hull. The hydrostatic force was calculated using the relative motion of the ship and the wave and an approximated underwater volume. When a section exited the water, a slamming force was applied to the section upon reentry. Both Von Karman and Wagner slamming theories were tested, with Von Karman working better due to much of the bow having a relatively large deadrise angle. As a result, only the Von Karman results are shown here.

The added mass force was handled in one of two ways. Method 1 assumed that the added mass remained constant throughout the experiment. The estimated wet natural frequencies were then used to perform a time domain simulation. Method 2 used the dry natural frequencies and an added mass force modeled from impact theory, as given in Equation (8) [10], where c is the instantaneous half wetted beam, and $\dot{V}$ is the vertical acceleration.

$$F_z = \rho \frac{\pi}{2} c^2 \dot{V} \tag{8}$$

The results of the two different methods are shown in Figure 26 and Figure 27 for the 15 knots, 1/15 slope regular waves, head seas case. Method 1 (constant added mass) predicted the low frequency bending moment poorly, especially for hogging. The high frequency component was overpredicted in magnitude, and the frequency is shifted, resulting in poor matching of the time history. Method 2 (changing added mass) was closer in amplitude to the response, but still not accurate in the time history. Therefore, the simple models are not sufficient to predict the structural response of the model.

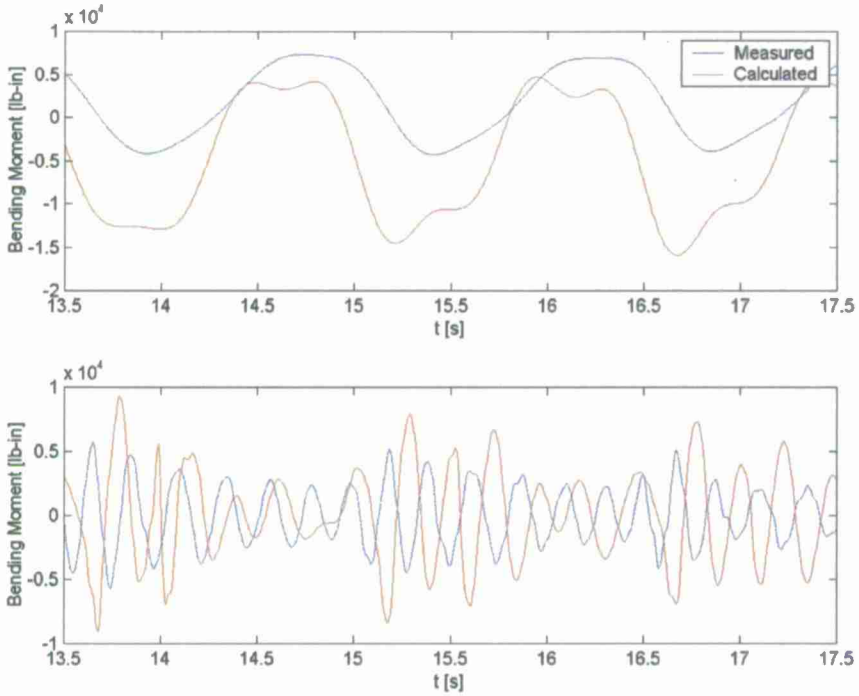

Figure 26. Low and high frequency components of midship bending moment for Run 478 using Method 1 where calculated bending moment uses constant estimated added mass.

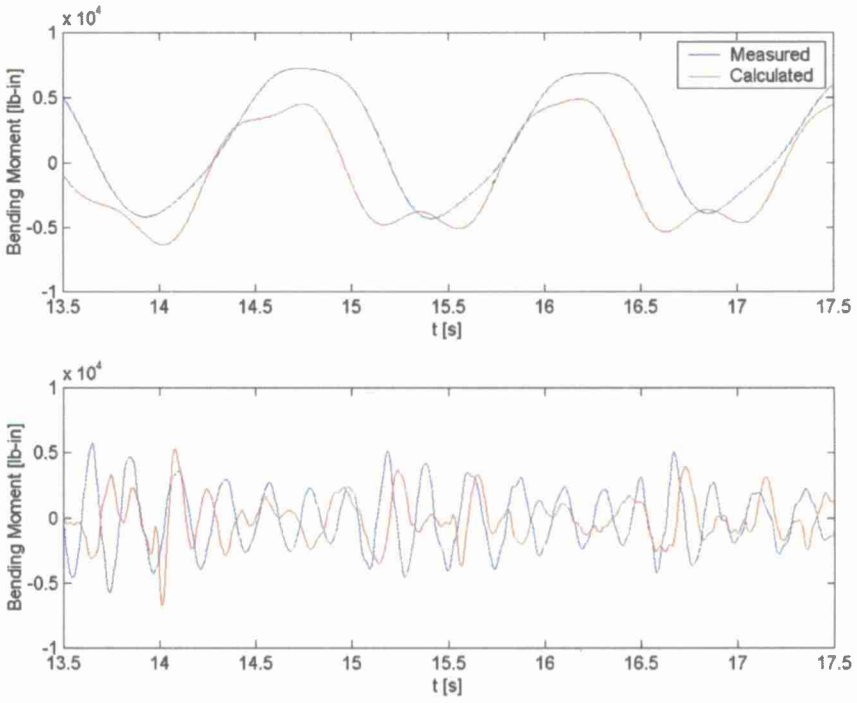

Figure 27. Low and high frequency components of midship bending moment for Run 478 using Method 2 where calculated bending moment uses changing added mass from impact theory.

For non-linear systems, initial conditions are very important and even small changes in initial conditions can cause large changes in response. There are two difficulties in determining initial conditions for each impact event and subsequent whipping response. The first difficulty is determining the time at which to take the initial conditions. There are no pressure sensors directly at the bow to measure wave impacts there. The closest pressure gauges are just over 0.066L aft of the forward perpendicular, while the closest slam panel is 0.125L aft of the forward perpendicular. Therefore, the time that an impact event begins must be extrapolated from the time one of the other sensors registers the impact. The slam panel G1 (15 inches or 0.125L aft of the forward perpendicular) is used for this study. The second difficulty is determining which initial conditions are important for the problem. For a single degree of freedom system, the initial position and velocity will determine the response, however, for a continuous system, the important parameters are not so clear. Another problem is in filling the parameter space for the initial conditions. This lack of a complete set of initial conditions makes determining basins of attraction near impossible. Figure 28 shows an initial condition plot for all events for conditions of 15 knots, 1/15 regular wave, head seas cases and 25 and 35 knot 1/30 regular wave cases. The scatter of points shows how difficult it is to make any definitive statement on the role of initial conditions on the whipping response.

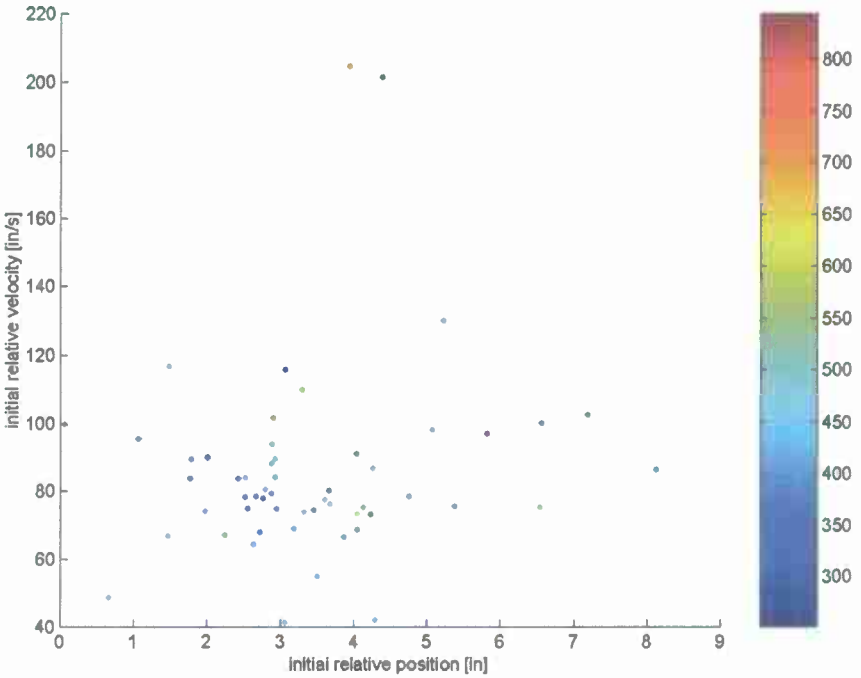

Figure 28. Whipping response amplitude (in-lbs, shown on colorbar) versus initial relative position and velocity of FP.

CONCLUSIONS

The JHSS Segmented Monohull Model seakeeping tests provided a large data set for validation of numerical tools. The motions and loading predictions by LAMP showed good correlation with the experimental data. Additionally, NFA predictions of ship stability showed reasonable correlation with the experimental data. The study of the hydroelastic response of the JHSS model has revealed some important points. Springing does not appear to have a large effect on the loading of the vessel. The midship bending moment for irregular seas has a relatively small component at the lowest natural frequency of the model. The whipping response, on the other hand, can be significant. For some cases, the whipping response reaches nearly the same amplitude as the wave induced bending. This important phenomenon is also very complex, and therefore difficult to predict. Different methods of understanding and predicting the whipping response of the vessel had varying degrees of success, but ultimately could not adequately explain the results of the experiments, suggesting that more complex numerical simulations are likely necessary.

REFERENCES

[1] Devine, E. A., Turner, C. R., Bishop, R. C., & Amsden, J. (2007). *Preliminary, Quick-Look Results of Seakeeping and Structural Loads Tests Conducted for the Joint High Speed Sealift (JHSS) 1:47.53-Scale Segmented Ship Model (Model 5663).*

[2] Devine, Edward. "An Overview of the Recently-Completed JHSS Monohull and Trimaran Structural Seaways Loads Test Program." Presentation, 30 October 2009.

[3] Rottman, J. W., Brucker, K. A., Dommermuth, D. G., & Broutman, D. (2010). "Parameterization of the internal wave field generated by a submarine and its turbulent wake in a uniformly stratified fluid", *Proceedings 28th Symposium on Naval Hydrodynamics*, Pasadena, California, USA.

[4] Dommermuth, D. G., O'Shea, T. T., Wyatt, D. C., Ratcliffe, T., Weymouth, G. D., Hendrikson, K. L., Yue, D. K., Sussman, M., Adams, P., & Valenciano, M. (2007). "An application of cartesian-grid and volume-of-fluid methods to numerical ship hydrodynamics", *Proceedings of the 9th International Conference on Numerical Ship Hydrodynamics*, Ann Arbor, Michigan.

[5] O'Shea, T. T., Brucker, K. A., Dommermuth, D. G., & Wyatt, D. C. (2008). "A numerical formulation for simulating free surface hydrodynamics", *Proceedings of the 27th Symposium on Naval Hydrodynamics*, Seoul, Korea.

[6] Brucker, K.A., O'Shea, T.T., Dommermuth, D.G., & Adams, P. (2010). "Three dimensional simulations of Deep-Water breaking waves", *Proceedings of the 28th Symposium on Naval Hydrodynamics*, Pasadena, California, USA.

[7] Ratcliffe, T., Minnick, L., O'Shea, T., Fu, T., Russell, L., and Dommermuth, D. (2008). "An integrated experimental and computational investigation into the dynamic loads and free-surface wave-field perturbations induced by head-sea regular waves on a 1/8.25 scale-model of the R/V Athena", *Proceedings of the 28th Symposium on Naval Hydrodynamics*, Seoul, Korea.

[8] Lewandowski, E. The Dynamics of Marine Craft, World Scientific, 2004.

[9] Troesch, A. W. (2008). *NA 440 Course Notes.* Ann Arbor, MI: Course Packs Plus.

[10] Faltinsen, O. M. (2005). *Hydrodynamics of High Speed Marine Vehicles.* New York, NY: Cambridge University Press.

This page intentionally left blank.

DISTRIBUTION LIST

Copies		Name
NAVSEA		
1		DTIC
Division Distribution		
1	3452	Library (pdf only)
1	5050	Thomas Fu (pdf only)
4	5830	Anne Fullerton, Craig Merrill, (pdf only), Files (2)
1	5510	Christopher Bassler (pdf only)
1	654	Allen Engle (pdf only)
ONR		
1		Paul Hess
SAIC		
4		Don Wyatt, Tom O'Shea, Kyle Brucker, Doug Dommermuth (pdf only)